B.2.2 Definition of RPVHPN Cracking Modes

This section introduces the spatial discretization used to model PWSCC in RPVHPNs and, subsequently, the different cracking modes modeled at the various locations. Each cracking mode reflects a cracking type observed on reactor vessel heads in industry. Due to varying geometry, accessibility, material condition, etc., each mode is modeled with a unique set of initiation, load, growth, and examination techniques. It is important to distinguish each mode, as they will be referenced frequently throughout this appendix. Table B-1 summarizes each mode. Figure B-4 provides a schematic of a general RPVHPN and indicates the primary growth direction (i.e., the direction that leads to leakage) of each modeled PWSCC mode.

For the purpose of this study, each RPVHPN is divided into an uphill and downhill side. Each cracking mode may initiate on either the uphill or downhill sides, both of which have their own unique loading conditions. The downhill and uphill sides are selected as the only circumferential locations for crack initiation. This convention is based on the fact that the downhill and uphill locations are the locations of highest tensile weld residual stresses (due to nozzle ovalization).

The key characteristics of the cracking modes modeled in this study are given below:

- **ID axial cracks (Mode 1)** – partial through-wall cracks located on the penetration nozzle ID. These cracks are conservatively assumed to initiate in the region above the weld such that they immediately result in leakage if they penetrate through-wall into the OD nozzle annulus. These cracks are opened by hoop stresses in the penetration nozzle.
- **OD axial cracks (Mode 2)** – partial through-wall cracks located on the penetration nozzle OD located below the weld. These cracks cause leakage if they grow in length to reach the nozzle OD annulus; they may transition to through-wall axial cracks if they grow through-wall before reaching the annulus. These cracks are opened by hoop stresses in the penetration nozzle.
- **Radially-oriented weld cracks (Mode 3)** – cracks located on the J-groove weld that grow toward the weld toe. These cracks cause leakage if they reach the weld toe. These cracks are opened by hoop stresses in the J-groove weld.
- **Through-wall axial cracks (Mode 4)** – through-wall cracks located below the weld. These cracks may only form if an OD axial crack reaches through-wall before reaching the nozzle OD annulus. These cracks cause leakage if they grow long enough to reach the nozzle OD annulus. These cracks are opened by hoop stresses in the penetration nozzle.
- **Circumferential through-wall cracks (Mode 5)** – through-wall cracks located on the weld contour above the weld. These cracks are assumed to occur immediately following leakage caused by any of the preceding crack modes, either by branching of the flaw causing the leakage or by initiation of a new flaw on the OD surface of the nozzle. These cracks are opened by a complex stress field acting orthogonally to the weld contour.

Table B-1
Summary of PWSCC Modes Modeled on RPVHPNs

Mode ID	Orientation	Shape	Material Characteristics	Location	Transitions to…
1	Axial	Semi-elliptical, part-through-wall	Alloy 600	Top of weld, inner diameter	Mode 5 upon growing through-wall
2	Axial	Semi-elliptical, part-through-wall	Alloy 600	Bottom of weld, outer diameter	Mode 5 upon growing to weld root, or mode 4 upon growing through-wall
3	Radially-oriented	Semi-elliptical, part-through-weld	Alloy 82/182	On weld	Mode 5 upon growing to weld root
4	Axial	Rectangular, through-wall	Alloy 600	Bottom of weld	Mode 5 upon growing to weld root
5	Circumferential	Through-wall	Alloy 600	Along upper weld contour	Ejection upon growing past stability threshold

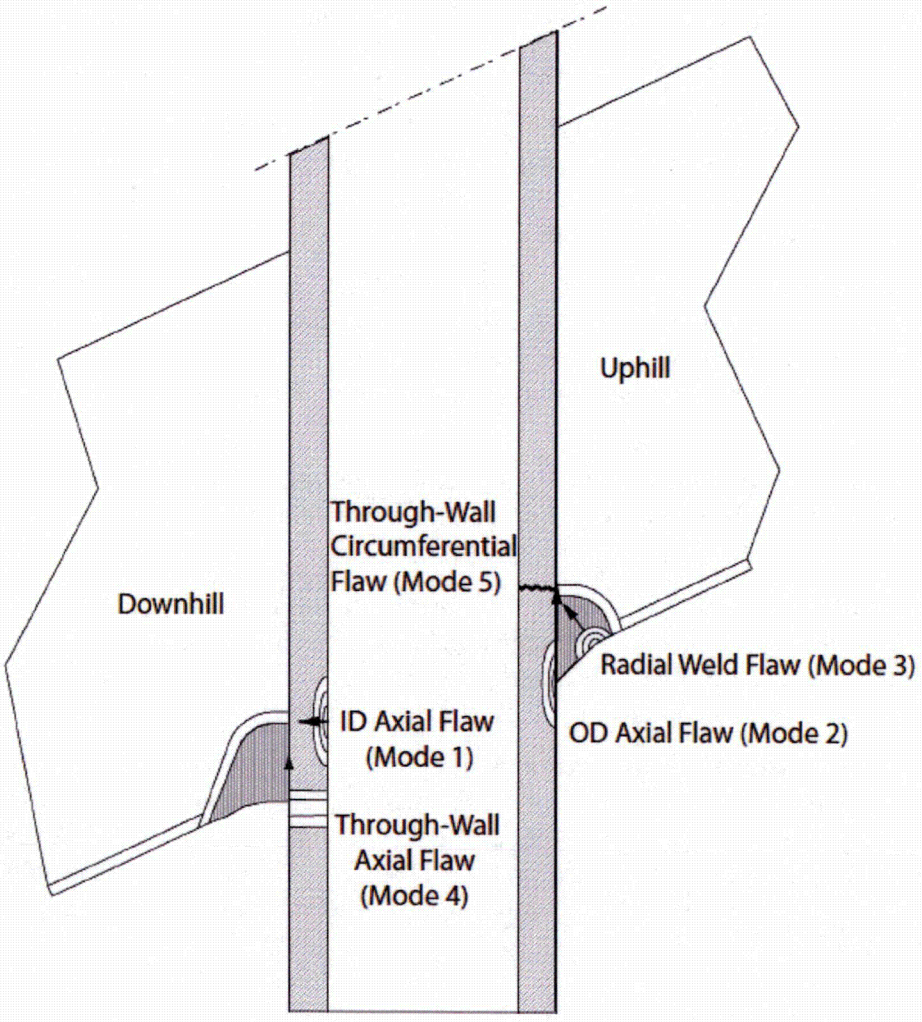

Figure B-4
Schematic of Modeled Cracking Modes for RPVHPN Probabilistic Assessment (Arrows Indicate Direction of Growth Toward Leakage)

B.3 Load and Stress Model

Load models are used to calculate stresses at the different locations of interest for PWSCC on RPVHPNs. The crack growth model uses this stress information; it is noted, however, that the RPVHPN crack initiation model does not explicitly account for stress dependence.

The load models account for welding residual stresses as well as operational loads. In addition, a peening residual stress model is introduced for modeling crack growth during cycles after a peening application, if applicable.

The methodologies for calculating stresses due to operational loads, penetration welding, and peening are discussed in Sections B.3.1, B.3.2, and B.3.3, respectively. Considerations for the effects of temperature and load cycling are discussed in Section B.3.4. The loads used for crack growth at the various locations are summarized in Section B.3.5.

B.3.1 Internal Pressure and Piping Loads

The operational stresses, which are due predominantly to internal pressure, are separated from the residual stresses in this analysis (as they were for the DM weld load models). This separation serves a practical purpose in modeling peening because it allows for peening effects to be applied to existing residual stresses, without altering operational stresses. The operational stresses can be superimposed with post-peening residual stresses to provide the total stresses used to estimate crack growth.

Unlike DM welds, the complex geometry of a reactor vessel head penetration precludes the accurate estimation of operational stresses at the various locations of interest by way of analytical, or textbook, approaches. Accordingly, operational stresses at each location have been ascertained from the results of various J-groove weld finite element analyses (the general methodology of such RPVHPN FEA studies is outlined in [6]). Specifically, operational stresses are attained by subtracting stress states predicted by FEA during operation from those predicted during shutdown (i.e., operational = total – residual).

Operational stress at each location of interest is treated as being constant through-wall (or through-weld), with a magnitude equal to the *surface* operational stress predicted by FEA results. This convention accurately accounts for the separation of residual and operational stresses near the peened surface. Careful separation of the residual and operational stresses away from the peened surface is not necessary; the total stress profile after peening is largely insensitive to the way residual and operational stresses are separated away from the surface (as becomes apparent after reviewing the peening modeling methodology in Section A.3.3).

The FEA results reveal that operational stresses are negligible at the OD and weld surfaces (in comparison to the welding residual stresses at these surfaces). As with DM welds, pressure acting to open a crack face is included after crack formation such that the operational stresses become:

$$\sigma_{oper,OD} = P$$
$$\sigma_{oper,weld} = P \qquad \text{[B-1]}$$

Hoop operational stresses at the ID surface are modeled using a stress concentration that is applied to the nominal hoop stress estimated with thin-walled cylinder theory:

$$\sigma_{oper,ID} = F_{oper,ID}\frac{PD_i}{2t} + P \qquad \text{[B-2]}$$

where $F_{oper,ID}$ is the ID hoop stress concentration factor, P is the normal operating pressure, D_i is the penetration nozzle inner diameter, and t is the penetration nozzle thickness. The ID stress concentration factor has been derived from FEA results as is detailed in Section B.8.1. Note that this equation also includes the pressure acting to open the crack face after crack formation.

B.3.2 Welding Residual Stress Before Peening

The J-groove welding residual stress profiles at six locations/directions (vectors) of interest are derived from the same set of FEA results used for operational stresses in the previous section. Specifically, six vectors are relevant for predicting the crack growth modes discussed in Section B.2.2: hoop stress from the penetration nozzle ID to the OD above the weld (uphill/downhill), hoop stresses from the penetration nozzle OD to the ID below the weld (uphill/downhill), and hoop stresses from the weld surface to the weld toe (uphill/downhill). These vectors are depicted in Figure B-5.

For all six vectors, a second-order polynomial function of through-wall (or through-weld) fraction is used to model the total stress profile. These polynomials are fit to FEA results during operational loading (and the residual stresses are attained by subtracting the operational stresses discussed in the previous section). This is different from the third- and fourth-order curves used for welding residual stresses in DM welds, but is considered accurate for capturing the essential gradient and curvature characteristics observed in RPVHPN FEA results [6]. The resulting general equation form is:

$$\sigma_{tot,loc}\left(\frac{x}{D}\right) = \sigma_{0,FEA,loc} + \sigma_{1,FEA,loc}\left(\frac{x}{D}\right) + \sigma_{2,FEA,loc}\left(\frac{x}{D}\right)^2 + P \qquad \text{[B-3]}$$

where the *loc* subscript is a placeholder for the various locations of interest, D is a general dimension equal to the penetration nozzle thickness for ID and OD locations and equal to the weld path length for weld locations, and $\sigma_{0,FEA,loc}$, $\sigma_{1,FEA,loc}$, and $\sigma_{2,FEA,loc}$ are sampled parameters based on curve-fits to FEA results. Note that the standard superposition approach is applied to consider the crack face pressure by adding it to the membrane stress term in the equation above.

The fit parameters are calculated such that they give the second-order polynomial stress profile defined by the following three points:

1. The stress at the initiation surface:

$$\sigma_{tot,loc}(0) = \sigma_{0,FEA,loc} + P \qquad \text{[B-4]}$$

2. The stress at the opposite surface (or the weld root for weld locations):

$$\sigma_{tot,loc}(1) = R_{1,loc}\sigma_{0,FEA,loc} + P \quad [B\text{-}5]$$

3. The stress at the mid-radius (or the mid-point between the weld center and the weld root for weld locations):

$$\sigma_{tot,loc}(0.5) = R_{0.5,loc}\left(\frac{\sigma_{0,FEA,loc} + R_{1,loc}\sigma_{0,FEA,loc}}{2}\right) + P \quad [B\text{-}6]$$

The $R_{1,loc}$ and $R_{0.5,loc}$ terms are indicative of the average gradient and curvature of the resulting stress profile, respectively. Together with the surface stress at the location/direction of interest ($\sigma_{0,WRS,loc}$), these terms have been fit to FEA results, as detailed in Section B.8.1.

For completeness, the general welding residual stress equation is given below:

$$\sigma_{WRS,loc}\left(\frac{x}{D}\right) = \sigma_{0,FEA,loc} + \sigma_{1,FEA,loc}\left(\frac{x}{D}\right) + \sigma_{2,FEA,loc}\left(\frac{x}{D}\right)^2 - \sigma_{oper,loc} \quad [B\text{-}7]$$

B.3.3 Residual Stress After Peening

As discussed previously, peening has the effect of adding a thin region of compressive stress in all three principal directions near the surface of its application. This compressive region both prevents crack initiation and slows the growth of cracks (especially short cracks), and hence peening is required to be captured in this modeling effort.

At all locations of interest for each penetration, the peening effect is modeled in the same manner as in the DM weld program (see Section A.3.3); i.e., using a four-region piecewise equation that combines a compressive region near the surface with the pre-existing residual stresses while maintaining the same equivalent force through-wall (or through-weld) before and after peening. For that reason, the details of peening modeling will not be repeated here. Any differences in the way peening is applied in the DM weld program and the RPVHPN program are noted below:

- For RPVHPNs, the initial compressive surface stress and the penetration depth are sampled independently at each location. This is different from the DM weld program, which assumes that the peening is applied uniformly to all ID locations.
- For RPVHPNs, the compressive residual stress depths are sampled from separate distributions for the ID locations, as compared to the OD and weld locations. A peening compressive residual stress depth of 1.0 mm is assumed for the wetted nozzle OD and surface attachment area susceptible to PWSCC initiation, whereas a compressive residual stress depth of 0.25 mm is assumed for the nozzle inside surface. These assumptions are based on the peening performance criteria defined in Section 4.
- For weld locations, the through-element dimension is the weld path length instead of the penetration nozzle thickness (i.e., in Equations [A-18] through [A-21]).
- The effect of peening on growth is conservatively neglected for several scenarios described below:

- ID peening stresses above the weld are assumed to have no effect on the growth of circumferential through-wall cracks. The growth of circumferential through-wall cracks is based on stress intensity factors that were calculated with finite element software and these models did not include stresses representative of a peened nozzle.
- OD peening stresses below the weld are assumed to have no effect on the growth of partial through-wall axial OD cracks that have grown under the weld far enough that the upper crack surface tip is outside of the peening compressive layer (as demonstrated in Figure B-6).
- ID peening stresses do not affect nearly through-wall axial OD cracks (as demonstrated in Figure B-6), i.e., the thin compressive region near the ID is not given credit for abating the growth of mostly (90-100%) through-wall cracks.

B.3.4 Effect of Operating Temperature and Load Cycling

Residual stress relaxation due to temperature and load cycling can occur at penetration locations, as it can in DM weld components. As discussed for DM welds, the effects of thermal relaxation and load cycling (i.e., shakedown) must be considered when demonstrating that the minimum peening stress effect required by the applicable performance criteria will be obtained. Thus, the effects of thermal relaxation and load cycling subsequent to peening of RPVHPNs are implicitly addressed through modeling of the bounding stress effect meeting the performance criteria in the calculations of this appendix.

B.3.5 Summary of Load Model

The RPVHPN load model is used to attain through-wall (or through-weld) stress profiles on the different vectors that are attributed to the growth of the various cracking modes.

Total stresses and operational stresses (i.e., those stresses due to loads present during operation) are derived from FEA results and welding residual stresses are attained from the difference between the total and operational stresses. The total stress profile at each location is modeled with a second-order polynomial function of the through-wall fraction. The operational stress profile at each location is modeled with a constant stress.

Prior to peening, the total stress profiles used to predict crack growth are those derived from FEA results (plus the crack face pressure contribution).

The peening load model modifies the welding residual stress profiles to predict post-peening residual stresses. After peening is applied, the post-peening residual stress profile is superimposed with the operational stresses to attain the total stress profiles used to predict crack growth.

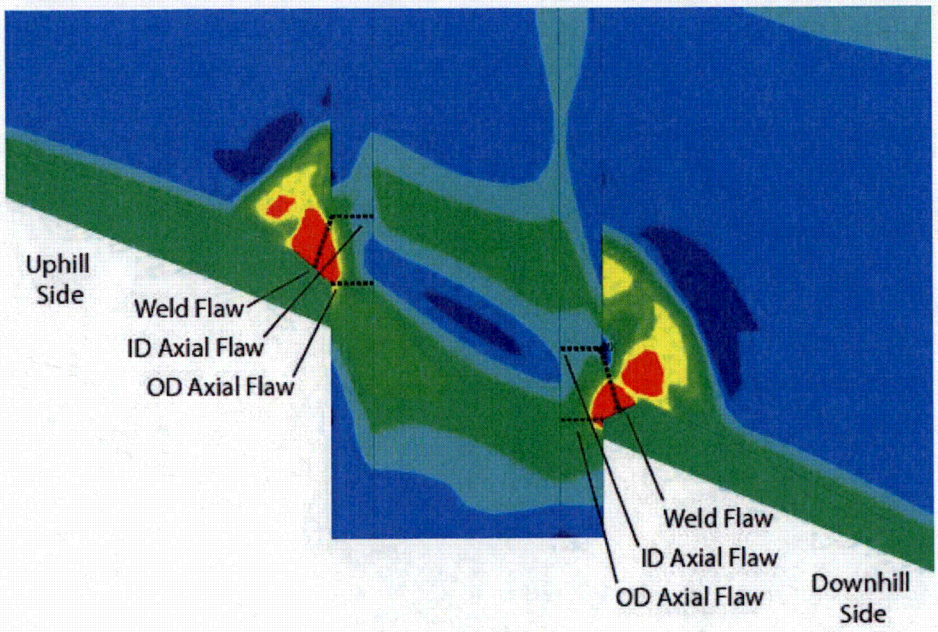

Figure B-5
Depiction of Stress Profile Vectors for Each Crack Mode Location (six bold dotted lines) and Welding Residual Hoop Stress Contour Plot

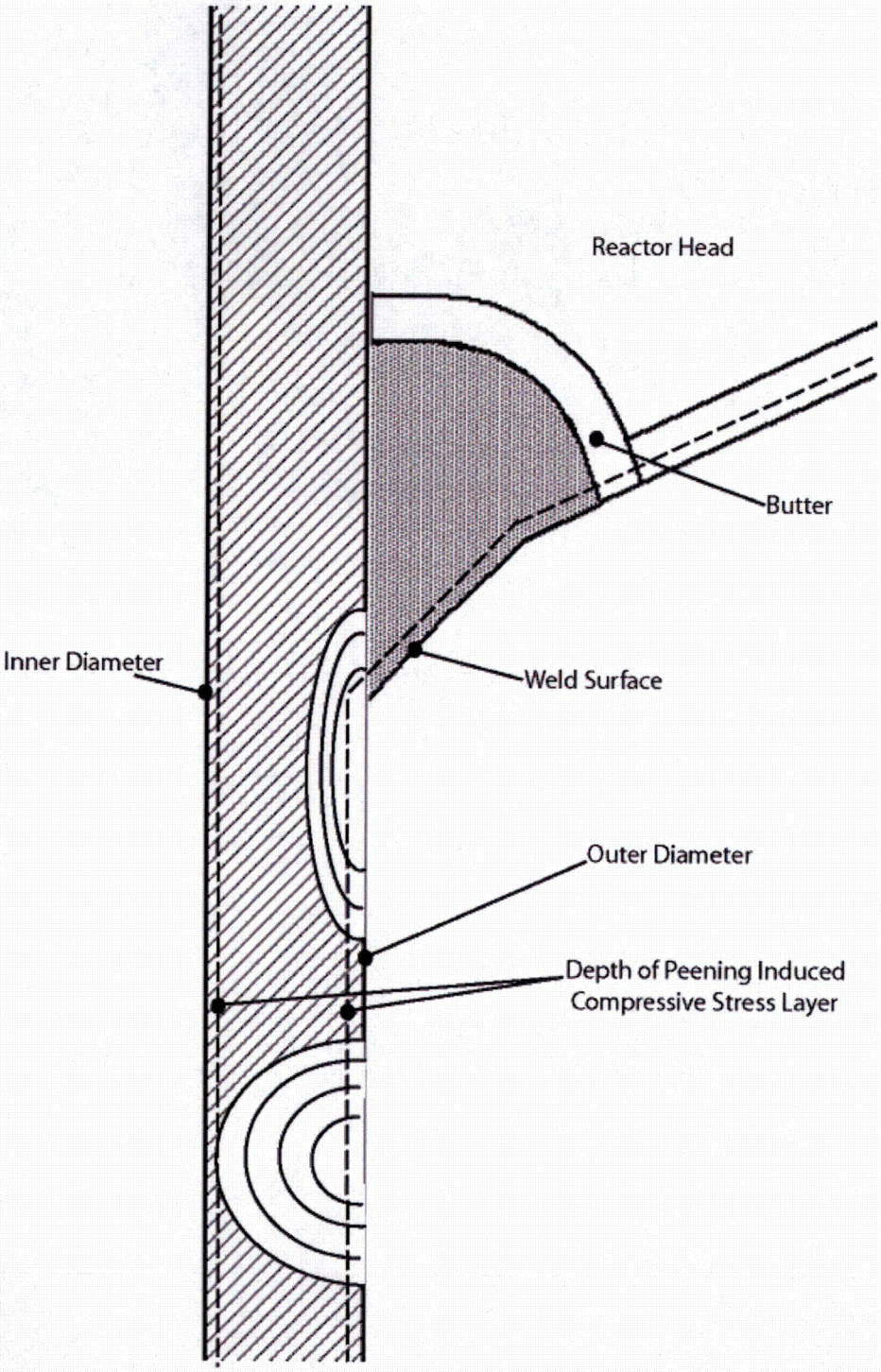

Figure B-6
Scenarios for Excluding Peening Effects in RPVHPNs: a) Crack Extends Below Weld, Past Compressive Stress Layer (top flaw); b) OD Crack Depth Reaches ID Compressive Stress Layer (bottom flaw)

B.4 Crack Initiation Model

This study employs a statistical Weibull approach for predicting crack initiation that is similar to the approach used by the DM weld program (discussed in Section A.4). As such, much of the information presented for DM welds will not be repeated in this section, which will instead focus on detailing the differences between the initiation models.

The key difference in the initiation models is that the RPVHPN initiation model does not include a surface stress adjustment. This adjustment was considered unfounded for RPVHPNs based on the following information:

- The surface stresses at all RPVHPN locations of interest are randomly sampled and are similar in tensile magnitude while surface stresses at DM weld locations vary systematically as a function of distance from the point of maximum tensile bending stress. Accounting for this systematic stress variation on the DM weld circumference is important for modeling coalescence.
- No clear stress-dependent location preference emerges from industry experience of PWSCC initiation on RPVHPNs.
- There is no known precedent for applying a stress-adjustment when modeling initiation of PWSCC on RPVHPNs.

A second notable difference is that the RPVHPN initiation model predicts PWSCC initiation across all of the penetrations in a single head, as opposed to a single component.

B.4.1 Spatial Discretization of Crack Sites

The spatial discretization of the crack locations is described in Section B.2.2. To summarize, six cracking modes are considered for crack initiation in this study: axial cracks on the nozzle ID at the top of the weld (uphill/downhill), axial cracks on the nozzle OD at the bottom of the weld (uphill/downhill), and radially-directed cracks at center of the weld surface (uphill/downhill).

These six *locations* are considered for the number of penetrations in the head, N_{pen}, resulting in $6N_{pen}$ total initiation *sites*.

In this appendix, the subscript *loc* is used to denote the different locations and the subscript *i* is used to denote the different penetrations on the head.

B.4.2 Initiation Time of First Crack

As was done to predict time of first initiation on DM welds, a Weibull model has been selected for predicting the time of first initiation of PWSCC in RPVHPNs. The use of this statistical model reflects systematic and statistical variations in material properties and environmental conditions from head to head, across the industry. The advantages of the Weibull model, and a general description, can be found in Section A.4.2.

The Weibull slope, β, an arbitrary failure fraction, F_1, (e.g., 0.1%, 1%, 10%, 63.2%, etc.), and the time at which this arbitrary failure fraction is reached, t_1, are provided as inputs to the probabilistic model. The value of the Weibull characteristic time parameter, θ, is then determined during runtime using Equation [A-30]. The process by which β, F_1, and t_1 are fit to existing data for first crack initiation in RPVHPNs is discussed in Section B.8.2.

Once β and θ are known for the current Monte Carlo realization, they can be used to sample a reference initiation time in EDY (t_{ref}). The sampled initiation time is adjusted for temperature (to convert to EFPY) using the Arrhenius relationship:

$$t_f = t_{ref} \times e^{\left(\frac{Q}{R}\right)\left(\frac{1}{T}-\frac{1}{T_{ref}}\right)} \qquad \text{[B-8]}$$

The result of the above equation is considered to be the *average* time of the first PWSCC initiation for the head. Unlike the DM weld initiation model, this time is not applied to any specific initiation site. Similar to the DM weld initiation model, this time is used by the multiple crack initiation model, which is discussed next.

B.4.3 Initiation Times of Multiple Cracks

A Weibull model has been selected for use in predicting times of initiation of multiple PWSCC cracks on a head. The use of this statistical model reflects systematic and statistical variations in material properties and environmental conditions from location to location, and from penetration to penetration, on a single head.

The multiple crack initiation Weibull model uses a separate Weibull slope, $\beta_{mult,i}$, to reflect a new rate at which PWSCC degradation spreads to multiple sites on a head after the first crack initiation. This Weibull slope is sampled for each penetration to reflect the premise that each penetration has unique conditions relevant to multiple flaw initiation[13]. The distribution selected for $\beta_{mult,i}$ is discussed in Section B.8.2.

Since the time provided by Equation [B-8] is indicative of the average time of the first PWSCC initiation across all $6N_{pen}$ crack sites, it is therefore associated with the cumulative probability (F_{1st}) given in Equation [B-9] below:

$$F_{1st} = \frac{1-0.3}{6N_{pen}+0.4} \qquad \text{[B-9]}$$

For each penetration, the characteristic time parameter for the multiple flaw Weibull model, $\theta_{mult,i}$, is calculated from $\beta_{mult,i}$, t_{ref}, and F_{1st} above using Equation [A-30]. Then, an initiation time for each crack site, $t_{ref,i,loc}$, is sampled from the resulting Weibull distribution. Sampled initiation times are not truncated at t_{ref} as they were for DM welds.

The above approach allows for the initiation of multiple cracks and it can be shown that, on average, a single initiation across all initiation sites is expected prior to t_{ref}, the average time of first initiation based on industry experience.

[13] It is noted that sampling the multiple flaw Weibull slope for each penetration results in the clustering of flaws on affected penetrations. This clustering effect may have a strong impact on leakage and ejection probabilities due to the detection, repair, and stability logic. In a sensitivity study, the Weibull slope will only be sampled for each reactor vessel head to demonstrate the relative effect of the sampling strategy.

B.4.4 Crack Initialization

Crack initialization refers here to assigning initial conditions to each crack at its initiation time. These initial conditions include size, location, and capacity for growth. The crack modes are fixed by the initiation site, as discussed in Section B.4.1.

Initial crack depth is sampled from a distribution of positive, non-zero, crack depths. This reflects both that the Weibull initiation models discussed above were fit to industry data recording first detection of crack indications and that crack detection is only possible for finite crack sizes. Initial crack lengths are attained by scaling the initial depth by a sampled aspect ratio.

Initiation location is not tracked for ID cracks. ID cracks are assumed to initiate at an arbitrary axial location near the weld top such that leakage occurs upon through-wall growth. Similarly, weld cracks are assumed to initiate at the weld center.

Initiation location is tracked for OD cracks. The variability in OD crack axial location affects the crack's susceptibility to leakage; i.e., the OD crack location together with the OD crack length provides a means to predict if the crack has grown long enough to reach the nozzle OD annulus. For OD cracks, the initial axial location is attained by taking a uniform sample between the weld toe and the axial location where the weld residual surface stress falls below 80% of yield stress. For a typical Alloy 600 penetration nozzle, this results in an initiation location threshold of approximately 30-40 ksi. This threshold is larger than the 20 ksi presumed to be required for PWSCC initiation [7], but conservatively results in initiation locations nearer to the OD nozzle annulus. Furthermore, crack initiation locations are likely to be biased toward the higher stress region. The location of 80% of yield was derived from results of J-groove welding residual stress FEA results [6].

In a similar fashion to the DM weld initialization, the capacity for growth of each crack is dependent on sampled crack growth variation terms: f_{weld} and $f_{ww,i}$ for Alloy 82/182 cracks or f_{heat} and $f_{wh,i}$ for Alloy 600 cracks. The accepted tendency of components that are more susceptible to PWSCC initiation to have higher flaw propagation rates can be included by correlating the sampled f_{weld} and f_{heat} terms with the average time of first initiation, t_{ref}.

B.5 Crack Growth Model

The RPVHPN crack growth model is similar to the DM weld model in many regards. Namely, both models allow the prediction of PWSCC growth rate as a function of crack geometry, component loading, and other conditions. However, the RPVHPN includes more conditionality due to the various different PWSCC locations and modes (e.g., Alloy 600 vs. Alloy 82/182, ID vs. OD, etc.) and the fact that cracking is modeled beyond through-wall crack growth such that ejection can be predicted.

This section details the model augmentation required to make growth predictions of the RPVHPN cracking modes. The new methods for the calculation of stress intensity factors, which are the result of new crack and component geometries, are presented in Sections B.5.1 through B.5.4. The rate equations for crack growth in Alloy 600 are presented in Section B.5.5. Section B.5.6 discusses other special considerations made for predicting growth given the geometry characteristics specific to a RPVHPN component. Section B.5.7 discusses the special

considerations made for predicting growth given a stress profile characteristic of a peened component (i.e., with a compressive stress region near the surface).

B.5.1 Stress Intensity Factor Calculation Using Influence Coefficient Method

The influence coefficient method for the calculation of stress intensity factor is presented in detail in Section A.5.1. This method assumes that the stress profile acting orthogonally to the crack face (i.e., hoop stresses for the cracking modes of interest in this study) is defined by a polynomial function in the direction of crack depth and is uniform along the crack length. The first of these two conditions is upheld prior to peening provided the second-order polynomial stress profiles described in Equation [B-7]. The second condition, stress profile uniformity along the crack length, is not upheld in reality due to the rapidly changing residual stress distributions near the J-groove weld. For modeling purposes, the stress results extracted from FEA on the approximate vectors shown in Figure B-5 are assumed uniform over the crack face; as can be observed from the hoop stress contour plot, these vectors tend to lie over more severe stress magnitudes, for the respective crack type.

The general form of the stress intensity factor calculation, for a second-order stress profile, by way of the influence coefficient method is:

$$K = \left[\sigma_0 G_0 + \sigma_1 G_1 \left(\frac{a}{D} \right) + \sigma_2 G_2 \left(\frac{a}{D} \right)^2 \right] \sqrt{a\pi} \qquad \text{[B-10]}$$

where the G terms are the influence coefficients specific to the crack and component geometries and the location on the crack. Once again, D is a general dimension equal to the penetration nozzle thickness for ID and OD locations and equal to the weld path length for weld locations.

The influence coefficients for ID and OD crack locations are interpolated from tables built by way of finite element parametric analyses. In the DM weld study, lookup tables were used for ID, semi-elliptical, surface cracking (Tables 15 and 39 of Marie, et al. [8]). Tables 16 and 44 of Marie, et al. [8] provide lookup tables for OD, semi-elliptical, surface cracks. Interpolation and extrapolation of these tables use the criteria presented in Table A-1.

The calculation of stress intensity factors for weld cracks is not as clear as for the ID or OD crack locations. This is because there are no pre-determined influence coefficient lookup tables for cracks with the unique boundary conditions of the J-groove weld. As an approximation, cracks at the weld locations are treated as being on a flat plate with a thickness equal to the head thickness, t_{head}. Under this assumption, the influence coefficients may be interpolated from either the ID or OD lookup tables, using an R_i/t lookup value of 1000 and a through-wall fraction lookup value of a/t_{head}. For an R_i/t ratio value of 1000, both the ID and OD solutions have asymptotically converged to the solution for a flat plate.

B.5.2 Stress Intensity Factor Calculation Using Weight Function Method

After peening, the stress profile cannot be defined accurately by a polynomial function in the through-wall direction so the more versatile weight function method is used to calculate stress intensity factors.

The weight function method is fully detailed for calculating stress intensity factors of DM weld cracks in Section A.5.2. Since the methodology outlined in that section adequately covers stress intensity factor calculation at RPVHPN locations, no new information is given here.

B.5.3 Stress Intensity Factor Calculation for Through-Wall Axial Cracks

If an axial OD crack goes through-wall prior to reaching the nozzle OD annulus, growth continues in the length direction. In this case, the semi-elliptical crack shape assumed in Sections B.5.1 and B.5.2 breaks down and a through-wall model is required to accurately predict stress intensity factor at the crack tips.

Marie, et al. [8] provides an influence coefficient method for the prediction of stress intensity factor of a rectangular through-wall crack. The influence coefficient equation is:

$$K = \sigma_m F_m \sqrt{c\pi} \qquad \text{[B-11]}$$

where c is the half-length of the through-wall crack, σ_m is the membrane elastic stress, and F_m is the lone influence coefficient.

In this study, the membrane elastic stress is approximated as the through-wall average of the total stress profile, attained by taking the analytical integral of the total stress polynomial. It is noted that this value does not change after peening because of the peening force balancing term; as a corollary, peening does not act to slow the growth of through-wall axial cracks in this study.

The influence coefficient is interpolated from a lookup table using the following dimensionless parameter:

$$\lambda = \frac{c}{\sqrt{R_m t}} \qquad \text{[B-12]}$$

where R_m is the mid-radius of the penetration nozzle.

Table 35 of Marie, et al. [8] provides an FEA-based lookup table spanning values of λ from 0.2 to 5.0. Conservatively, for the rare case that a crack occurs with a value of λ less than 0.2, the stress intensity factor for λ=0.2 is used. Values of λ greater than 5.0 do not occur for typical RPVHPN geometries because at this size these hypothetical cracks will have reached the nozzle OD annulus resulting in a leak and a transition to the circumferential through-wall crack.

B.5.4 Stress Intensity Factor Calculation for Through-Wall Cracks on the Weld Contour (i.e. Circumferential Cracks)

In the RPVHPN probabilistic analysis, any crack predicted to leak is assumed to transition immediately to a through-wall crack along the J-groove weld contour. The growth of such cracks is required to be modeled until the nozzle ejection criterion is reached.

Because of the oblique growth direction of these cracks, and the complex stress profile along the length of the crack, there exists no parameterized method for predicting stress intensity factors at the crack tips as a function of the stress distribution characteristics (as has been done for all

previous K calculations). Instead, stress intensity factors are predicted as a function of crack length exclusively, using FEA results.

References [9] and [10] describe finite element analyses performed to predict stress intensity factors at the tips of through-wall cracks growing along the contour of RPVHPN J-groove welds, from both the uphill and downhill sides of the nozzle, at various elevations. These analyses include effects of welding residual stress and operational loads. Both analyses use the geometry of the outermost nozzle at the subject plant, resulting in a generally bounding welding residual stress profile along the crack face.

Across these studies, the most bounding average K versus crack length curves have been selected for use in this probabilistic analysis (those from Reference [10]). Figure B-7 shows these K curves, for the uphill and downhill sides of the nozzle. Linear interpolation is used between FEA evaluated points. (Extrapolation is never necessary because these cracks are modeled initiate at 30°, and ejection of the nozzle is modeled to occur at 300°, as will be discussed in forthcoming sections.)

Conservatively, the K curves presented in Figure B-7 are used for all through-wall cracks along the J-groove weld contour, regardless of the penetration angle of the nozzle being simulated.

Finally, although the analyses in References [9] and [10] are state-of-the-art, and are expected to give relatively accurate results in comparison to similar analyses performed in the nuclear industry, there still exists large uncertainty given welding process variation and plant-to-plant geometry variation. To include this uncertainty, a distributed variable, $K_{circ,mult}$, may be used to scale the circumferential through-wall crack K curves. The distribution selected for this variable is discussed in Section B.8.3.2.

B.5.5 MRP-115 Crack Growth Rate Model for Alloy 82/182 (weld) and MRP-55 Crack Growth Rate Model for Alloy 600 (tube)

The model selected in this study to estimate PWSCC crack growth in the Alloy 82/182 weld metal is the same model presented in MRP-115 [11]. This model is fully described in Section A.5.3 for DM welds and accordingly is not represented here.

The model selected in this study to estimate PWSCC crack growth in the Alloy 600 base metal is based on CGR data presented in MRP-55 [12]. This model uses the same equation form as the Alloy 82/182 crack growth rate model:

$$\frac{\delta}{\delta t}(d) = e^{\frac{Q_g}{R}\left(\frac{1}{T}-\frac{1}{T_{ref}}\right)} \alpha f_{heat} f_{wh} \left(K_I - K_{Ith}\right)^b \qquad \text{[B-13]}$$

where d is a general crack dimension (e.g., depth or length). The time-stepping procedure used to solve for RPVHPN crack growth is identical to the one presented for DM welds.

Some of the empirical parameters for Alloy 600 growth differ from those applied to Alloy 82/182 growth and those in MRP-55; specifically, these are the power-law coefficient α, the crack-tip stress intensity factor threshold K_{Ith}, and the stress intensity factor exponent b. Section B.8.3 presents the derivation of these parameters based on Alloy 600 data.

The additional factors, f_{heat} and f_{wh}, are used to describe the aleatory uncertainty in the Alloy 600 crack growth rate model. The within-heat variation, f_{wh}, is a value sampled for each flaw site from a distribution reflective of the growth rate variation observed in laboratory studies of cracks in a controlled Alloy 600 specimen. Similarly, the heat-to-heat growth rate variation, f_{heat}, is a value sampled for each reactor vessel head from a distribution reflective of the growth rate variation observed in laboratory studies of cracks in identically controlled Alloy 600 specimens, after accounting for the within-heat variation. Section B.8.3 describes derivation of these distributions.

The sampled heat-to-heat variation terms may be correlated with the average time of first initiation to simulate the premise that heads that are more susceptible to PWSCC initiation tend to have higher flaw propagation rates.

Finally, for circumferential through-wall cracks growing along the weld contour, a distributed variable, $c_{mult,circ}$, is used to scale the growth rate predicted using Equation [B-13]. This distributed variable is intended to capture the possibility of the growth rate being accelerated by the concentrated chemical environment that may develop in the annulus on the nozzle OD above the weld. The potential for chemical concentration in the annulus is discussed in MRP-55 [12]. The distribution selected for this variable is discussed in Section B.8.3.2.

B.5.6 Special Considerations for Crack Growth on RPVHPNs

This section discusses the special constraints and interactions applied to the various cracking modes modeled for RPVHPNs. Similar to DM welds, these constraints and interactions are imposed by a set of modeling "rules" used to approximate known physical behaviors. While these physical behaviors are complex in nature, the simple set of rules is applied in the probabilistic model in order to capture the most essential growth characteristics.

Axial ID cracks are not given any particularly special modeling considerations. As discussed, these cracks are assumed to initiate at the top of the weld, grow until through-wall, and subsequently transition to the weld contour through-wall growth model.

Axial OD cracks are assumed to initiate below the weld, somewhere between the weld toe and the point where surface stress falls below 80% of yield. If the upper crack tip of an axial OD crack reaches the weld root, i.e., the nozzle OD annulus, the crack transitions to the circumferential through-wall crack model. If the crack depth penetrates through-wall prior to reaching the nozzle OD annulus, the crack transitions to the through-wall axial crack model. The axial through-wall crack transitions to the circumferential through-wall crack model once the upper crack tip reaches the nozzle annulus.

Weld cracks are assumed to initiate at the center of the J-groove weld and grow under the influence of hoop stresses in the weld until reaching the weld root (i.e., nozzle annulus); at this point, the crack transitions to the circumferential through-wall crack model. Weld crack lengths are constrained from growing past the half-width of the weld—the width of the weld half-way along the weld path line as demonstrated in Figure B-8.

As mentioned several times previously, leakage of any crack is immediately followed by the formation of a through-wall crack growing along the J-groove weld contour. The crack is assumed to initiate with a length equivalent to 30° around the weld contour. This assumption has a precedent in MRP-105 [5] and, together with the immediate transition to through-wall growth

on the weld contour after leakage, is expected to result in conservative estimates for the time to ejection following leakage.

The program considers the rare case where through-wall crack growth along the weld contour initiates on both the uphill and downhill sides of the penetration nozzle. In this case, the lengths of the uphill and downhill cracks are combined to assess for nozzle ejection (as detailed in Section B.7).

B.5.7 Special Considerations for Crack Growth on a Peened Surface

The special considerations made for predicting growth in a component with a stress profile characteristic of a peened component (i.e., with a compressive stress region near the surface) are the same as those expressed for a DM weld component in Section A.5.5: accounting for crack closure and "balloon" growth. The strategies used to account for these effects on RPVHPN cracks are identical to those used on DM weld cracks.

Separate sensitivity studies are presented later to demonstrate the relative effect of the crack closure and "balloon" growth on ejection probability of RPVHPNs.

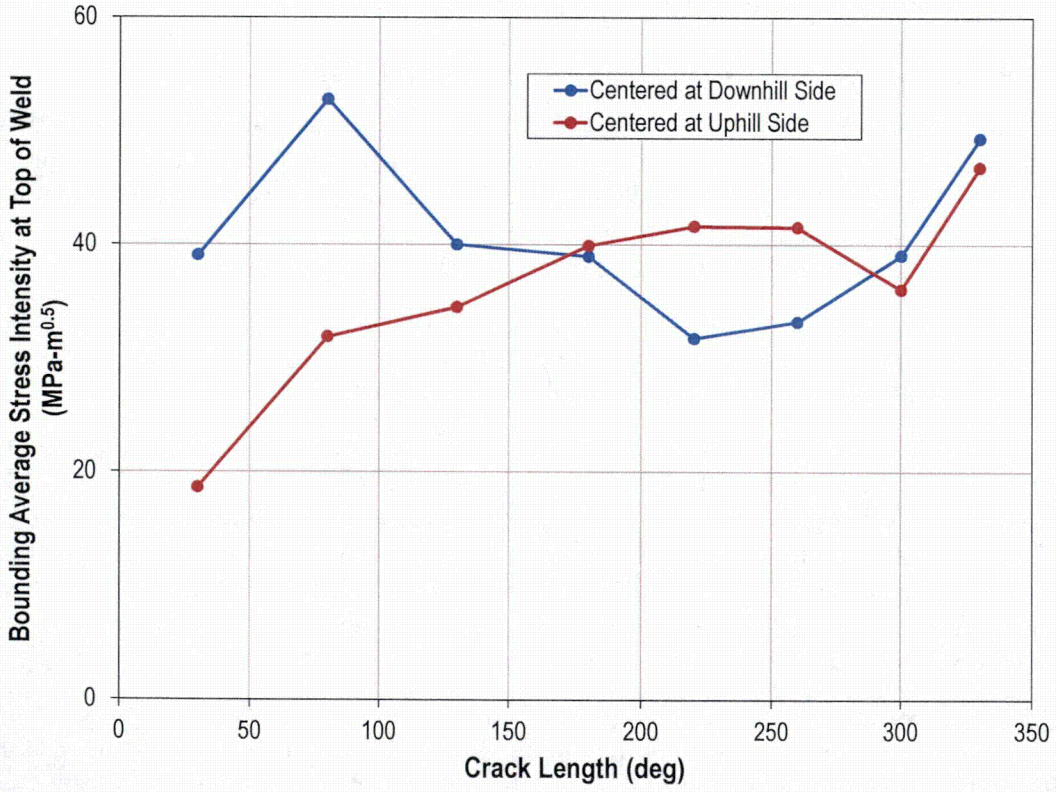

Figure B-7
Modeled Average Stress Intensity Factor vs. Crack Length for a Through-Wall Crack along the J-Groove Weld of a RPVHPN [10]

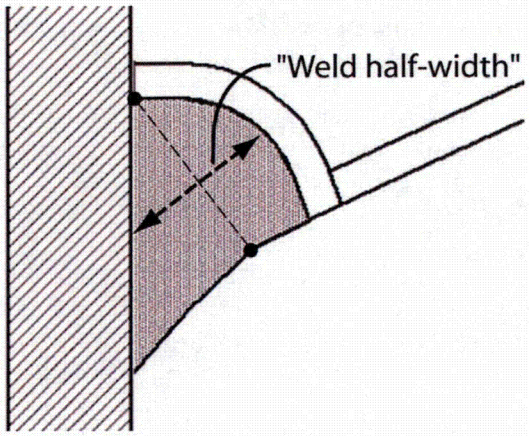

Figure B-8
Description of Weld Half-Width

B.6 Examination Model

This section describes the models applied to simulate ultrasonic and visual examinations of RPVHPNs.

Section B.6.1 discusses how examinations are scheduled, before and after peening, Section B.6.2 describes the inspection models, i.e., how POD is modeled, accounting for the geometry of the crack. Finally, Section B.6.3 describes the detection and repair modeling rules.

B.6.1 Examination Scheduling

UT inspection intervals for unmitigated RPVHPNs (e.g., prior to peening) are based on ASME Code Case N-729-1 [4], which gives the maximum number of operating cycles that are permitted between non-visual non-destructive examinations (NDEs) as a function of operating head temperature, cycle length, and capacity factor. The time of the first modeled UT inspection is set by the user.

Bare metal visual (BMV) inspection intervals for RPVHPNs are also based on N-729-1, which gives the VE (visual examination) interval as a function of the plant's effective degradation years (EDY). The first modeled BMV inspection is scheduled at the same outage of the first modeled UT inspection.

When peening is applied, different examination scheduling requirements and options are included in the model. First, during the peening application outage, immediately prior to peening, a UT inspection can be conducted to simulate a pre-peening inspection.

A follow-up UT examination is included before entering the relaxed in-service inspection (ISI) schedule. In this study, the follow-up inspection performed either one, two, three, or one and two cycles after the peening application for hot heads and either one, two, or three cycles after the peening application for cold heads.

After the follow-up examination, a new ISI schedule is used. The central goal of this probabilistic modeling effort is to demonstrate that the ISI inspection interval after peening can be relaxed, compared to N-729-1 requirements, without increasing the cumulative probability of

leakage and ejection over the entire plant service life. Accordingly, several different ISI intervals will be trialed after peening and compared to operation without peening.

For the base case, BMV inspection intervals are performed per the schedule prescribed in Section 4. Additionally, several sensitivity cases explore relaxed BMV inspection schedules after peening.

B.6.2 Inspection Modeling

This section describes the inspection models (i.e., the determination of POD) for UT and BMV inspections. The coverage requirements for each examination technique are discussed in Section 4.

For DM welds, the POD curve used for UT examinations was the result of a rigorous experimental study. Given the drastically different radius and thickness of a typical penetration nozzle, the UT curve from the DM weld study is not considered applicable here. Instead, a more general POD model described is used for UT inspection modeling of RPVHPNs. Instead of using absolute dimension as the POD argument, through-wall fraction is used to incorporate the dependence of UT performance on both the depth of the crack and the thickness of the component, resulting in the following POD equation:

$$POD\left(\frac{a}{t}\right)=\begin{cases} 0 & 0\le\frac{a}{t}<0.1 \\ \dfrac{e^{\beta_{1,UT}+\beta_{2,UT}\ln\left(\frac{a}{t}\right)}}{1+e^{\beta_{1,UT}+\beta_{2,UT}\ln\left(\frac{a}{t}\right)}} & 0.1\le\frac{a}{t}\le 1 \end{cases} \qquad \text{[B-14]}$$

Section B.8.4.2 gives the through-wall fraction/POD pairings used to define the probabilistic UT inspection curves for penetration nozzles (i.e., to calculate $\beta_{1,UT}$ and $\beta_{2,UT}$).

Similarly to the DM weld POD model, a POD of zero is conservatively applied for cracks with depths less than 10% through-wall. The model also includes the ability to linearly extrapolate the POD between the origin, i.e. 0% POD for an infinitesimal crack, and the POD given by Equation [B-14] for a 10% through-wall crack; this option is invoked in a sensitivity case.

It is noted that UT detection of both axial and circumferential through-wall cracks is modeled using an effective crack depth equal to the penetration nozzle thickness, i.e., a through-wall fraction of 1.

It is assumed for the purpose of the probabilistic model that any flaws located exclusively in the J-groove attachment weld are not detectable by UT inspection performed from the ID of the nozzle. In reality, it is possible that flaws in the weld metal that extend close to the fusion line with the base metal might be detectable by the UT examination.

BMV inspections are given a constant POD of p_{BMV} for leaking penetrations (i.e., RPVHPN with through-wall cracking to the nozzle annulus).

B.6.3 Detection and Repair Modeling

After probabilities of detection for the various examination methods have been calculated, detection is modeled in the same probabilistic manner as described for DM welds in Section A.6.3, including the capability to correlate back-to-back component inspections.

Leaking nozzles are inspected with the BMV probability a single time, regardless of the number of leaking cracks present on the nozzle.

If a crack is identified on a penetration, before or after the crack leads to leakage, the entire penetration is considered to be repaired or removed from service. The reactor vessel head is assumed to stay in operation after this repair/removal.

Credit can be taken for the condition that the unit(s) of interest have had no flaw detections prior to some user-defined past inspection time. If the detection occurs before this user-defined past inspection time, the Monte Carlo realization for the head is rejected and repeated with newly sampled inputs.

B.7 Nozzle Ejection Criterion

At the end of each Monte Carlo realization, the probabilistic model discussed in this report stores a limited number of metrics related to the extent of flaw growth and the repair status of individual penetrations and the head as a whole, including the timing and cracking mode type of related events. Most importantly, during each realization, the code tracks if any penetration nozzle is ejected and, if so, the number of the cycle of the ejection.

Credit can be taken for the condition that the unit(s) of interest have had no nozzle ejections prior to some user-defined past inspection time. If a nozzle is predicted to eject before this user-defined past inspection time, the Monte Carlo realization is rejected and repeated with newly sampled inputs, and the ejection is not counted toward the metric discussed above.

The critical size for a through-wall crack on the circumference of a penetration nozzle is a user-defined constant, in degrees. The choice of critical size for penetration nozzle ejection is discussed in Section B.8.6.

It is noted that credit is taken for penetration nozzle incidence angle when converting crack length to degrees. Specifically, crack angle, Θ, is calculated by the following equation:

$$\Theta = \frac{2c}{2\pi R_m}\cos(\phi) \qquad \text{[B-15]}$$

where ϕ is the penetration nozzle incidence angle. It is noted that this results in a greater effective length for ejection for all nozzles with a non-zero penetration incidence angle.

B.8 Probabilistic Model Inputs

The RPVHPN probabilistic modeling framework takes both deterministic and distributed inputs. The values of the deterministic inputs are constant for every Monte Carlo realization. The values of the distributed inputs are determined by sampling probability distributions during each Monte Carlo realization.

The inputs selected for use in the probabilistic model are discussed in Section B.8.1 through B.8.5. Inputs for both hot and cold head base cases are included in Table B-2 through Table B-5 and Table B-8 through Table B-11. Input values are highlighted orange to indicate any differences between hot and cold heads.

B.8.1 Reactor Vessel Head Geometry, Operating Time, Temperature, and Loads

The choice of inputs for geometry, operating time, temperature, and loading are discussed in this section. These inputs are given for the two cases for which results will be presented: a hot and a cold head. There is currently a subpopulation of 24 reactor vessel top heads with Alloy 600 penetration nozzles operating in the U.S. Of these 24 heads, 19 operate at cold-leg temperature (i.e., cold heads) and five operate at a temperature significantly above cold-leg temperature (i.e., non-cold heads). The penetration nozzles of these heads are potential candidates for peening mitigation. The characteristics of these plants were incorporated to generate results in this report, inasmuch as possible. Namely, the hot head and cold head temperatures were selected to bound head temperatures from this subpopulation.

B.8.1.1 Component Geometry

The penetration nozzle wall thickness and outer diameter used for the hot and cold head are taken as deterministic inputs, assumed constant across penetration nozzles.

The nozzle thickness and OD that are applied for all hot head penetration nozzles are based on information provided in MRP-48 [1] for CRDM nozzles in Westinghouse-designed reactor vessel heads. ICI nozzles are modeled with the same geometries, despite the fact that, in reality, ICI nozzles have larger ODs and smaller thicknesses. This simplification is appropriate considering that indications of PWSCC have not been reported to date for any top head ICI nozzles ([3], [13]).

The nozzle thickness and OD that are applied for all cold head penetration nozzles are based on information provided in MRP-48 [1] for CRDM nozzles in Westinghouse and B&W heads.

The reactor vessel thickness for the hot and cold head is taken as 6.0 inches, a thickness that is representative of the heads in service.

The number of penetrations and the apportionment of penetration nozzle incidence angles are based on a specific hot head and on a specific cold head. For both the hot and cold heads, the number of penetrations includes all CRDM nozzles and is characteristic of heads with Alloy 600 nozzles in service in U.S. PWRs. A heat vent penetration is not included in this modeling effort.

As discussed in the modeling sections, crack initiation and growth are modeled through the J-groove weld region of the RPVHPNs. For various modeling aspects, some key J-groove weld geometries are required including: the distance from the weld toe to the weld root ("weld toe-to-root distance", the distance from the weld surface to the weld root ("weld path length"), and the weld width halfway along the weld path length ("weld half-width") as depicted in Figure B-8. The variation of these geometries across penetrations was incorporated by fitting normal distributions to inputs for various J-groove weld FEA studies [6] (which span different heads and

penetration locations), at the uphill and downhill locations separately.[14] An example of such a fit (i.e., for the uphill weld path length) is given in Figure B-9. Lower and upper truncation limits were set based on the extreme values from the FEA studies. The ratio of the weld path length and the weld half-width was found to be approximately constant across penetration nozzles and accordingly was treated as a deterministic input.

General RPVHPN geometry inputs are included in Table B-2 and weld geometry inputs are included in Table B-3.

B.8.1.2 Operating Time

The hot and cold heads are simulated from plant startup until shutdown. Shutdown is considered to occur approximately 60 years after startup (i.e., a 40-yr original license and a 20-yr license renewal). Cumulative statistics are provided at the end of plant operational service period.

Both heads are assumed to have a capacity factor of 0.97. This value is representative of U.S. PWRs. Both heads are simulated with 24-month operating cycles. Five 24-month operating cycles results in the full 10-year interval between repeat ISI examinations that is required for peened heads in Section 4.3.

As discussed in the modeling sections, credit can be taken for the fact that the simulated unit has not experienced ejections or repairs before a user-defined outage. Monte Carlo realizations that predict repairs or ejections before some user-defined outage are rejected and rerun with new samples. This option is not invoked for the baseline results presented in this report. Accordingly the cumulative probabilities and ejection frequencies that are presented are not conditioned on any assumption of no ejection or repair before some date, and can be thought of as applying to the general population of heads with characteristics similar to those defined in Table B-2.

A user-defined outage, before which it is assumed that no ejections or repairs have occurred, will be set in a sensitivity case for each of the hot and the cold heads. The statistics presented in these two cases apply conditionally to heads that have experienced no ejections or repairs to date, but otherwise have characteristics similar to those defined in Table B-2.

B.8.1.3 Temperature

The mean hot and cold head temperatures were selected to bound the nominal operating temperatures for hot and cold heads with Alloy 600 RPVHPNs in service at U.S. PWRs [3].

Variation in head temperature and measurement error is incorporated into the model by using a normal distribution with a standard deviation of 5°F.

B.8.1.4 Operational Loads

As discussed in the modeling section, operational stresses (i.e., those stresses due to operational pressures and thermal gradients) are required to be separated from welding residual stresses. Results of finite element analyses of J-groove welding residual stresses [6] were used to estimate

[14] Trends in the geometry characteristics as a function of penetration incidence angle were analyzed. The trends were not strong enough to justify their implementation in this study.

these operating stresses by subtracting the FEA-predicted stress state present during operation from the welding residual stress state.

The results of these analyses revealed that the penetration nozzle OD and weld surface stresses had a negligible contribution from operational loads.

At the penetration nozzle ID, the results of these analyses revealed a distribution on the hoop stress concentration factor, $F_{oper,ID}$, defined in Equation [B-2]. A normal distribution provides an adequate fit to describe the variation in this concentration factor across penetration locations, as demonstrated in Figure B-10.

B.8.1.5 Welding Residual Stresses

Welding residual stress profiles on six vectors of interest (shown in Figure B-5) on RPVHPNs were synthesized from the results of J-groove weld FEA analyses [6]. More accurately, curves were fit to the total stress profiles (operational plus residual) predicted by FEA analyses and the residual stresses are calculated during runtime by subtracting operational stresses from the total stress profiles.

Equation [B-3] describes the second-order polynomial form of the stochastic family of curves fit to the FEA results. The coefficients of each polynomial stress profile are solved for each Monte Carlo realization based on the constraint that the total stress curve must pass through sampled stresses at three locations: x/D=0, x/D=1, and x/D=0.5, where:

- x/D=0 is defined as the location where cracks are expected to initiate: the ID above the weld for ID axial cracks, the OD below the weld for OD axial cracks, or the weld surface center for weld cracks.
- x/D=1 is defined as the location toward which cracks are expected to grow in depth: the OD above the weld for ID axial cracks, the ID below the weld for OD axial cracks, or the weld root for weld cracks.
- x/D=0.5 is defined as being halfway between the previous two locations.

Equations [B-4] through [B-6] give parameterized equations for the stresses at x/D=0, x/D=1, and x/D=0.5. Uncertainty inherent in data, as well as the uncertainty due to unknown variation of missing data, is introduced by allowing distributed inputs for the parameters in these equations: the surface stress, $\sigma_{0,tot}$, the gradient quantifier, $R_{1,tot}$, and the curvature quantifier, $R_{0.5,tot}$.

For each location of interest, a semi-analytical, iterative procedure was used to derive parameter distributions that resulted in a family of stress profile curves that bound the data and provide an adequate excess of uncertainty. Fifty instances from each of these families of curves, overlaid on the FEA data, are shown for each location of interest in Figure B-11 through Figure B-16 (the median stress profile is shown with a dotted black line). The parameter distributions used to make these families of curves are summarized in Table B-4. Conservatively, a minimum of zero is used for all parameters to ensure tensile hoop stresses at the three interpolated depths.

Table B-2
Summary of General RPVHPN Inputs

Symbol	Description	Source	Units	Parameter Type	Hot Head Base Case	Cold Head Base Case
	Total number of trials	Convergence Study	# trials		1.00E+06	1.00E+06
	Number of operating cycles	Selected to yield desired cumulative operating time	# cycles		30	30
	Nominal cycle length	Upper end of cycle length of U.S. PWRs	years		2	2
CF	Operating capacity factor	Representative capacity factor for U.S. PWR	-		0.97	0.97
	Cycle of first UT inspection	Based on typical operating reactor service histories	Cycle number		10	10
	Pre-peening UT inspection interval	ASME Code Case N-729-1	# cycles		1	3
	Pre-peening BMV inspection interval	ASME Code Case N-729-1	# cycles		1	2
T	Operating temperature	Selected based on properties of units serving as characteristic hot/cold head	°F	type	Normal	Normal
				mean	605	561
				stdev	5	5
				min	575	520
				max	635	600
N_{pen}	Number of modeled penetrations	Selected based on properties of units serving as characteristic hot/cold head	-		78	78
N_{flaw}	Maximum number of part-depth flaws modeled per penetration	Selected to capture PWSCC locations and mechanisms observed in industry RPVHPNs	-		6	6
t	Nozzle thickness	Representative of CRDM nozzle thickness of units serving as characteristic hot/cold head	in.		0.62	0.62
D_o	Nozzle outer diameter	Representative of CRDM nozzle OD of units serving as characteristic hot/cold head	in.		4.00	4.00
t_{head}	Reactor head thickness	Representative of industry PWRs	in.		5.98	5.98

Table B-3
Summary of Weld Geometry Inputs

Symbol	Description	Source	Units	Parameter Type	Hot Head Base Case	Cold Head Base Case
	Representative length from weld surface to weld root, uphill	Inputs to finite element analyses of J-groove weld residual stresses; distribution considers various penetration geometries	in.	type	Normal	Normal
				mean	1.05	1.05
				stdev	0.18	0.18
				min	0.50	0.50
				max	1.70	1.70
	Representative length from weld surface to weld root, downhill	Inputs to finite element analyses of J-groove weld residual stresses; distribution considers various penetration geometries	in.	type	Normal	Normal
				mean	0.97	0.97
				stdev	0.23	0.23
				min	0.50	0.50
				max	1.70	1.70
	Representative length from weld toe to weld root, uphill	Inputs to finite element analyses of J-groove weld residual stresses; distribution considers various penetration geometries	in.	type	Normal	Normal
				mean	1.38	1.38
				stdev	0.30	0.30
				min	0.80	0.80
				max	2.90	2.90
	Representative length from weld toe to weld root, downhill	Inputs to finite element analyses of J-groove weld residual stresses; distribution considers various penetration geometries	in.	type	Normal	Normal
				mean	1.36	1.36
				stdev	0.37	0.37
				min	0.80	0.80
				max	2.90	2.90
	Ratio of weld path length to weld half-width, uphill	Inputs to finite element analyses of J-groove weld residual stresses; distribution considers various penetration geometries	-		1.62	1.62
	Ratio of weld path length to weld half-width, downhill	Inputs to finite element analyses of J-groove weld residual stresses; distribution considers various penetration geometries	-		1.24	1.24
	Incidence angles for penetrations	Selected based on properties of units serving as characteristic hot/cold head	degrees		Discrete List	Discrete List

Table B-4
Summary of Loading Inputs for RPVHPN Model

Symbol	Description	Source	Units	Parameter Type	Hot Head Base Case	Cold Head Base Case
P_{op}	Normal operating pressure	Representative of industry PWRs	ksi		2.248	2.248
$f_{oper,ID}$	Nozzle ID operating hoop stress concentration factor	Finite element analyses of operational stresses on CRDM nozzle; across various penetration angles	-	type	Normal	Normal
				mean	3.480	3.480
				stdev	0.729	0.729
				min	0.000	0.000
				max	7.850	7.850

Table B-4 (continued)
Summary of Loading Inputs for RPVHPN Model

Symbol	Description	Source	Units	Parameter Type	Hot Head Base Case	Cold Head Base Case
$\sigma_{0,tot,1}$	Total hoop stress at penetration ID above weld	Finite element analyses of operational stresses on CRDM nozzle; across various penetration angles	ksi	type	Normal	Normal
				mean	40.99	40.99
				stdev	7.34	7.34
				min	0.00	0.00
				max	85.02	85.02
$\sigma_{0,tot,2}$	Total hoop stress at penetration OD below weld, uphill	Finite element analyses of operational stresses on CRDM nozzle; across various penetration angles	ksi	type	Normal	Normal
				mean	53.78	53.78
				stdev	9.92	9.92
				min	0.00	0.00
				max	113.30	113.30
$\sigma_{0,tot,3}$	Total hoop stress at weld surface center, uphill	Finite element analyses of operational stresses on CRDM nozzle; across various penetration angles	ksi	type	Normal	Normal
				mean	59.97	59.97
				stdev	5.73	5.73
				min	25.60	25.60
				max	94.34	94.34
$\sigma_{0,tot,-1}$	Total hoop stress at penetration ID above weld, downhill	Finite element analyses of operational stresses on CRDM nozzle; across various penetration angles	ksi	type	Normal	Normal
				mean	43.18	43.18
				stdev	8.30	8.30
				min	0.00	0.00
				max	92.95	92.95
$\sigma_{0,tot,-2}$	Total hoop stress at penetration OD below weld, downhill	Finite element analyses of operational stresses on CRDM nozzle; across various penetration angles	ksi	type	Normal	Normal
				mean	67.08	67.08
				stdev	10.60	10.60
				min	3.47	3.47
				max	130.69	130.69
$\sigma_{0,tot,-3}$	Total hoop stress at weld surface center, downhill	Finite element analyses of operational stresses on CRDM nozzle; across various penetration angles	ksi	type	Normal	Normal
				mean	61.78	61.78
				stdev	5.77	5.77
				min	27.15	27.15
				max	96.42	96.42

Table B-4 (continued)
Summary of Loading Inputs for RPVHPN Model

Symbol	Description	Source	Units	Parameter Type	Hot Head Base Case	Cold Head Base Case
$R_{1,tot,1}$	Stress gradient quantifier at penetration ID above weld, uphill	Finite element analyses of J–groove weld residual stresses (14 independent analyses)	-	type	Normal	Normal
				mean	1.11	1.11
				stdev	0.24	0.24
				min	0.00	0.00
				max	2.55	2.55
$R_{1,tot,2}$	Stress gradient quantifier at penetration OD below weld, uphill	Finite element analyses of J–groove weld residual stresses (14 independent analyses)	-	type	Normal	Normal
				mean	0.84	0.84
				stdev	0.14	0.14
				min	0.00	0.00
				max	1.68	1.68
$R_{1,tot,3}$	Stress gradient quantifier at weld surface center, uphill	Finite element analyses of J–groove weld residual stresses (14 independent analyses)	-	type	Normal	Normal
				mean	0.89	0.89
				stdev	0.32	0.32
				min	0.00	0.00
				max	2.81	2.81
$R_{1,tot,-1}$	Stress gradient quantifier at penetration ID above weld, downhill	Finite element analyses of J–groove weld residual stresses (14 independent analyses)	-	type	Normal	Normal
				mean	0.60	0.60
				stdev	0.41	0.41
				min	0.00	0.00
				max	3.06	3.06
$R_{1,tot,-2}$	Stress gradient quantifier at penetration OD below weld, downhill	Finite element analyses of J–groove weld residual stresses (14 independent analyses)	-	type	Normal	Normal
				mean	0.51	0.51
				stdev	0.13	0.13
				min	0.00	0.00
				max	1.29	1.29
$R_{1,tot,-3}$	Stress profile curvature quantifier at weld surface center, downhill	Finite element analyses of J–groove weld residual stresses (14 independent analyses)	-	type	Normal	Normal
				mean	0.36	0.36
				stdev	0.17	0.17
				min	0.00	0.00
				max	1.38	1.38

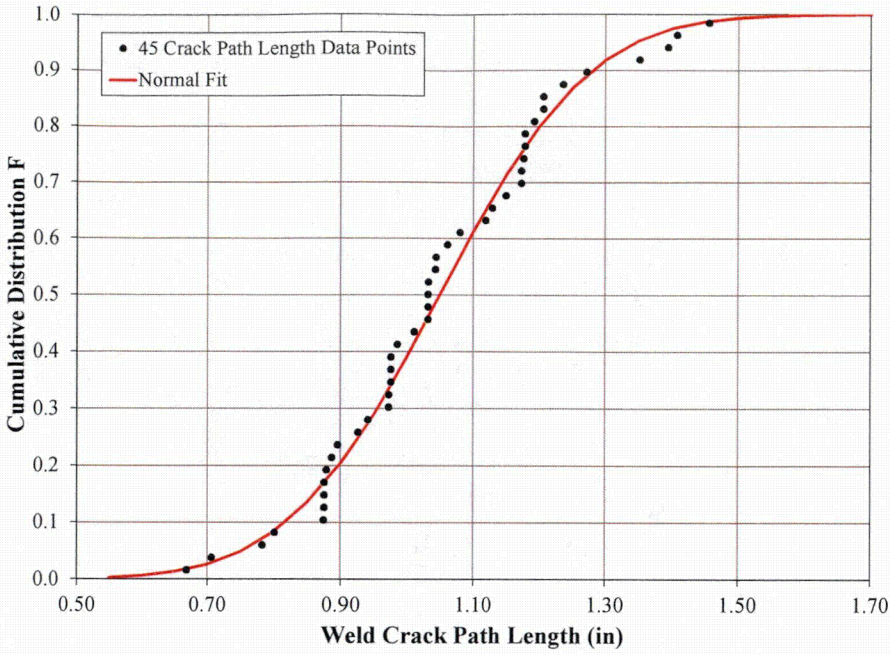

Figure B-9
Normal Distribution Fit to Geometry Data Varying Across Penetration Nozzle Incidence Angles: Uphill Weld Path Length

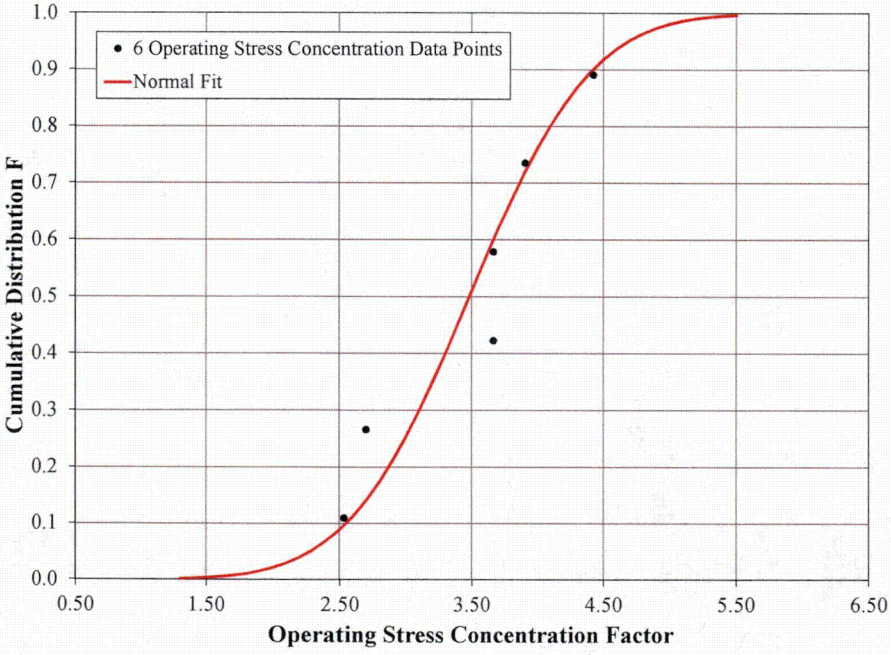

Figure B-10
Normal Distribution Fit to Penetration Nozzle ID Hoop Stress Concentration Factors Predicted by FEA Study

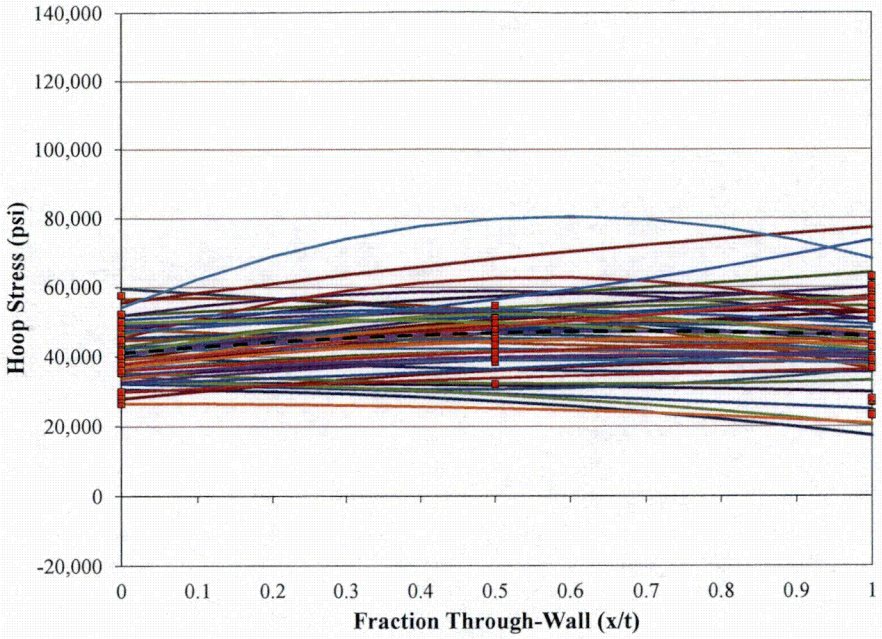

Figure B-11
Stochastic Family (50 instances) of Curves and FEA Results for the Total Stress Profile between the Penetration Nozzle ID Above the Weld and the Penetration Nozzle OD Above the Weld, Uphill Side

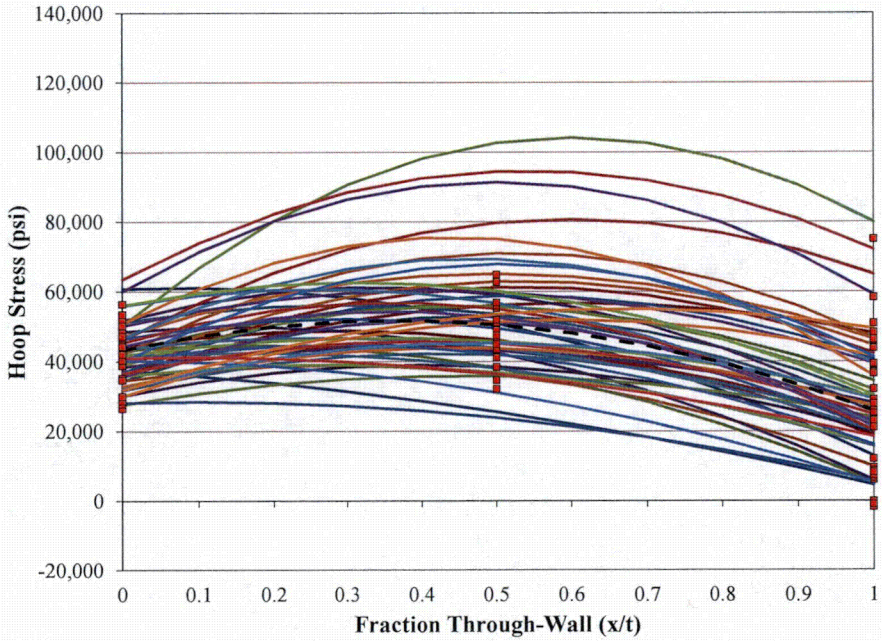

Figure B-12
Stochastic Family (50 instances) of Curves and FEA Results for the Total Stress Profile between the Penetration Nozzle ID Above the Weld and the Penetration Nozzle OD Above the Weld, Downhill Side

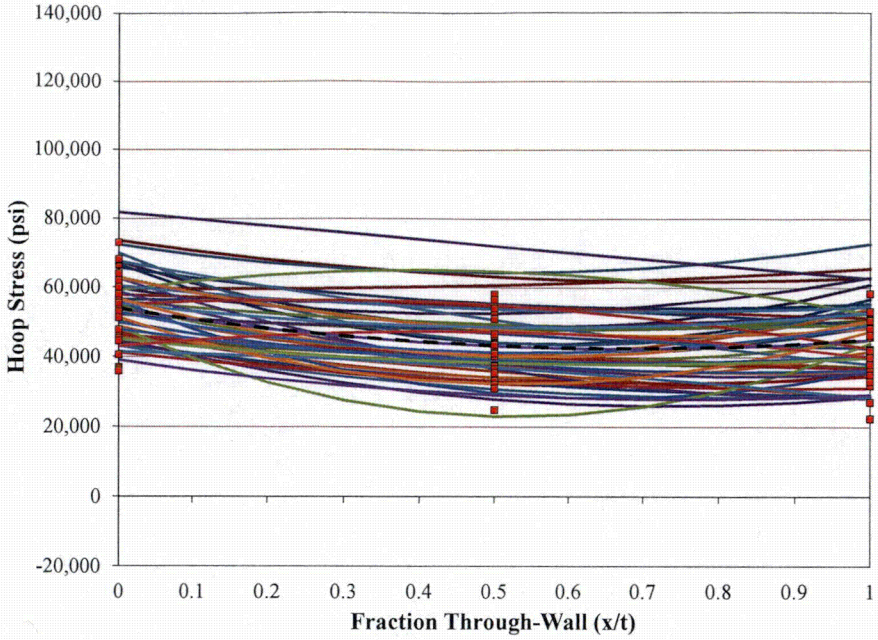

Figure B-13
Stochastic Family (50 instances) of Curves and FEA Results for the Total Stress Profile between the Penetration Nozzle OD Below the Weld and the Penetration Nozzle ID Below the Weld, Uphill Side

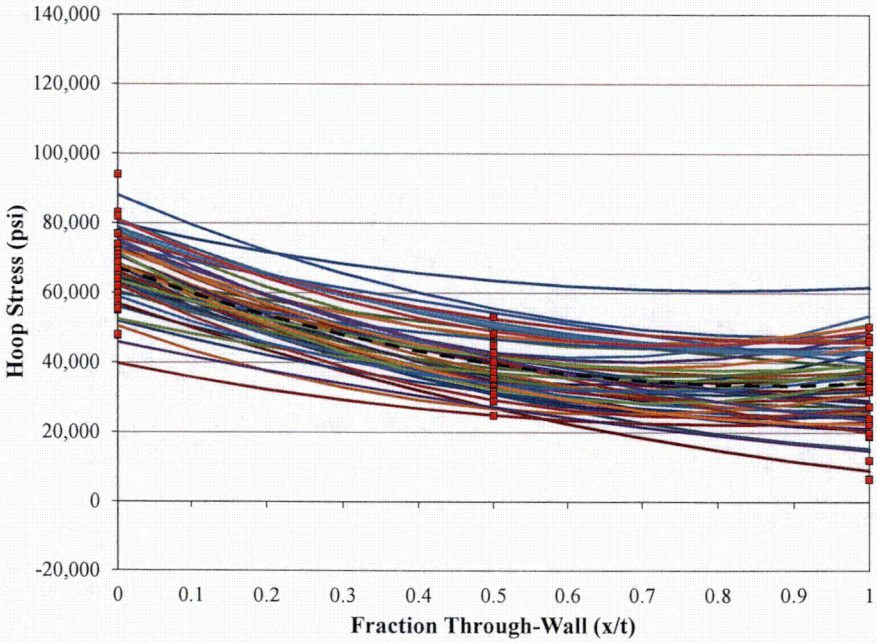

Figure B-14
Stochastic Family (50 instances) of Curves and FEA Results for the Total Stress Profile between the Penetration Nozzle OD Below the Weld and the Penetration Nozzle ID Below the Weld, Downhill Side

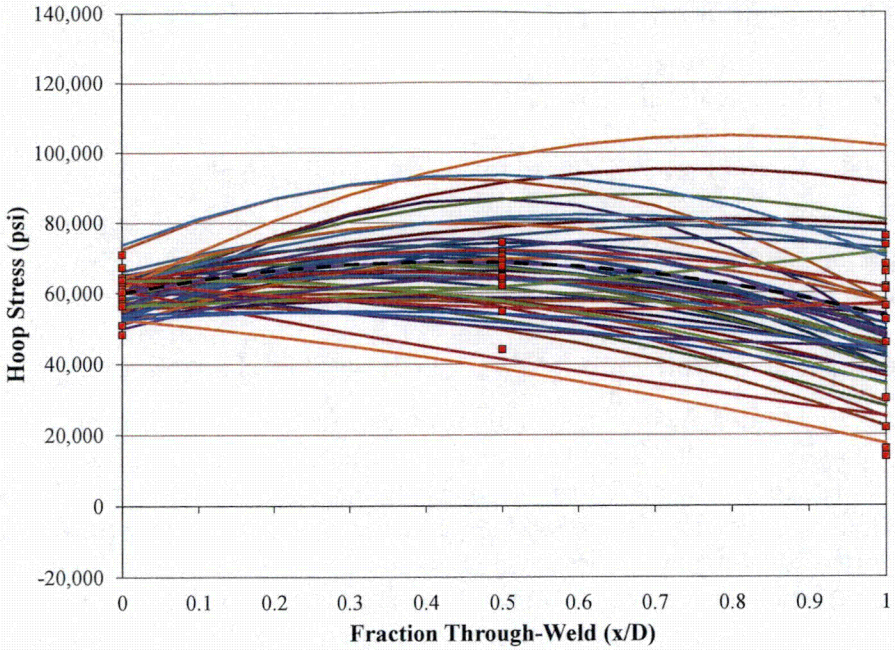

Figure B-15
Stochastic Family (50 instances) of Curves and FEA Results for the Total Stress Profile between the Weld Center and the Weld Root, Uphill Side

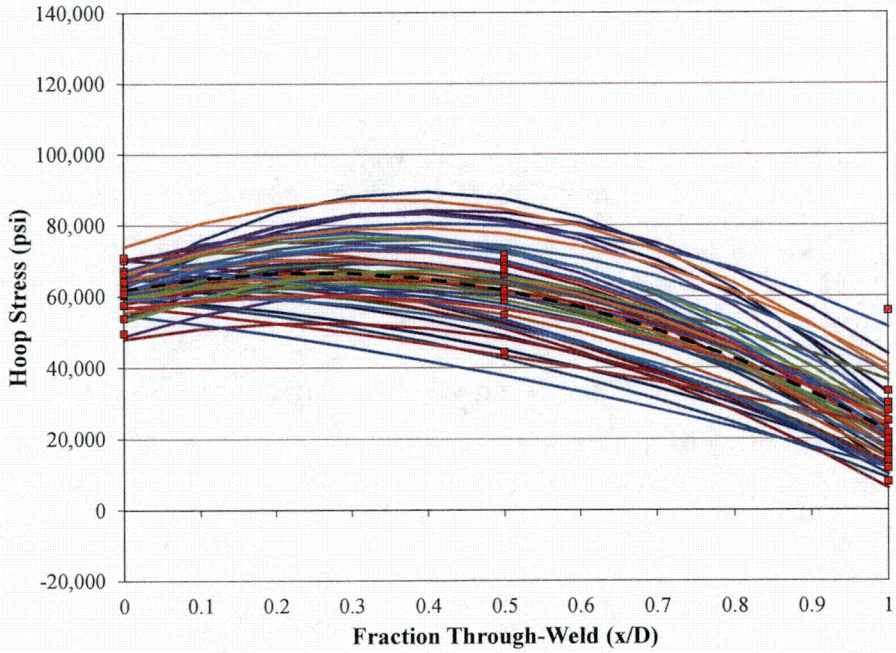

Figure B-16
Stochastic Family (50 instances) of Curves and FEA Results for the Total Stress Profile between the Weld Center and the Weld Root, Downhill Side

B.8.2 Crack Initiation Model

The set of inputs for the RPVHPN PWSCC initiation model is described in Table B-5 at the end of this section. Various inputs are detailed in the following subsections.

B.8.2.1 Industry Inspection Data used to Develop Initiation Model

Plant inspection data for RPVHPNs fabricated from Alloy 600 with J-groove welds fabricated from Alloys 82 and 182 were evaluated by DEI in MRP-395 [3]. Table B-6 lists the RPVHPNs in which cracking indications were detected that were used in this report.

B.8.2.2 Weibull Fitting Procedure for Average Time of First Initiation

The procedure used to fit a Weibull model to the time of first PWSCC initiation on a head differed from the like procedure for a DM weld, as presented in Section A.8.2. This is principally due to the fact that, generally, more than one cracking indication was discovered on heads during inspection, whereas inspection data for DM welds demonstrate only single cracking indications. In order to estimate the time of the first crack initiation on a particular head, a multiple flaw Weibull slope needed to be assumed; a value of 3.0 was chosen [3]. After the time of first PWSCC initiation on each head was estimated, the Weibull model was determined using a least squares fitting procedure.

B.8.2.3 Analysis Results for Average Time of First Initiation

Figure B-17 shows an example MLE Weibull distribution fit to the industry experience with RPVHPNs fabricated from Alloy 600 with welds from Alloys 82 and 182 given in Table B-6. The failure and suspension times were adjusted to a common reference temperature of 315°C (600°F) using a thermal activation energy of 184 kJ/mole (44 kcal/mole) (the mean value given in B.8.2.10). Table B-7 summarizes the MLE fit parameters of the Weibull analysis. Also included in Table B-7 are the standard errors in the Weibull fit parameter, β, and the vertical intercept of the linearized Weibull curve (which is used to determine the value of θ).

It is noted that the standard error in the vertical intercept of the linearized Weibull fit (referred to here as σ_c) is presented because it is used during runtime to account for the uncertainty in the value of the anchor point time, t_1.

B.8.2.4 Uncertainty in First Initiation Time Weibull Slope

A constant value for the Weibull slope, β, is applied to the initiation model. Uncertainty in the time to cracking is incorporated in the Weibull intercept parameter,[15] as discussed in Section B.8.2.5.

[15] The Weibull intercept parameter (the product of the Weibull slope parameter and the natural log of the Weibull characteristic time parameter) is the y-intercept of the "linearized" equation that results after log-transforming the Weibull cumulative distribution function twice. This linearization is a common practice in Weibull modeling because it poses the relationship between failure fraction and time in a linear form, which is useful for visualization and regression.